



1   **Validation of ash optical depth and layer height retrieved from**  
2   **passive satellite sensors using EARLINET and airborne lidar**  
3   **data: The case of the Eyjafjallajökull eruption.**

4

5   D. Balis<sup>1</sup>, M. E. Koukoulis<sup>1</sup>, N. Siomos<sup>1</sup>, S. Dimopoulos<sup>1</sup>, L. Mona<sup>2</sup>, G. Pappalardo<sup>2</sup>, F. Marengo<sup>3</sup>,  
6   L. Clarisse<sup>4</sup>, L. J. Ventress<sup>5</sup>, E. Carboni<sup>6</sup>, R. G. Grainger<sup>6</sup>, P. Wang<sup>7</sup>, N. Theys<sup>8</sup> and C. Zehner<sup>9</sup>

7

8   <sup>1</sup>Laboratory of Atmospheric Physics, Aristotle University of Thessaloniki, Greece,  
9   \*Email:balis@auth.gr

10

11   <sup>2</sup>Consiglio Nazionale delle Ricerche, Istituto di Metodologie per l'Analisi Ambientale (CNR-  
12   IMAA), Tito Scalo, Potenza, Italy

13

14   <sup>3</sup>Met Office, Exeter, United Kingdom

15

16   <sup>4</sup>Université Libre de Bruxelles, Brussels, Belgium

17

18   <sup>5</sup>National Centre for Earth Observation, Atmospheric, Oceanic and Planetary Physics,  
19   University of Oxford, United Kingdom

20

21   <sup>6</sup>COMET, Atmospheric, Oceanic and Planetary Physics, University of Oxford, United Kingdom

22

23   <sup>7</sup>Royal Netherlands Meteorological Institute (KNMI), De Bilt, The Netherlands

24

25   <sup>8</sup>Belgian Institute for Space Aeronomy (IASB-BIRA), Bruxelles, Belgium

26

27   <sup>9</sup>European Space Agency, ESRI, Frascati, Italy

28

29   **Abstract**

30   The vulnerability of the European airspace to volcanic eruptions was brought to the attention  
31   of the public and the scientific community by the 2010 eruptions of the Icelandic volcano  
32   Eyjafjallajökull. As a consequence of this event ash concentration thresholds replaced the  
33   'zero-tolerance to ash' rule, drastically changing the requirements on satellite ash retrievals.  
34   In response to that, ESA funded several projects aiming at creating an optimal *End-to-End*  
35   *System for Volcanic Ash Plume Monitoring and Prediction*. Two of them, namely the SACS-2  
36   and SMASH projects, developed and improved dedicated satellite-derived ash plume and  
37   sulphur dioxide level assessments. These estimates were extensively validated using ground-  
38   based and aircraft lidar measurements. The validation of volcanic ash levels and height  
39   extracted from the GOME-2 and IASI instruments on board the MetOp-A satellite is presented  
40   in this work. EARLINET lidar measurements are compared to different satellite retrievals for  
41   two eruptive episodes in April and May 2010. Comparisons were made between satellite



1 retrievals and aircraft lidar data obtained with UK's BAe-146-301 Atmospheric Research  
2 Aircraft (managed by the Facility for Airborne Atmospheric Measurements, FAAM) over the  
3 United Kingdom and the surrounding regions. The validation results are promising for most  
4 satellite products and are within the estimated uncertainties of each of the comparative  
5 datasets, but more collocation scenes are needed to perform a comprehensive statistical  
6 analysis. The satellite estimates and the validation data sets are better correlated for high ash  
7 optical depth values, with correlation coefficients greater than 0.8. The IASI data show a better  
8 consistency concerning the ash optical depth and ash layer height when compared with the  
9 lidar data.

10

## 11 **1. INTRODUCTION**

12 The Eyjafjallajökull volcano in Iceland (63.63°N, 19.62°W) erupted on the 14<sup>th</sup> of April 2010  
13 and the ash-loaded plume rose to more than 10 km, deflected to the east by westerly winds  
14 [Stohl et al., 2011]. The plume persisted from the 15<sup>th</sup> and the 26<sup>th</sup> of April 2010, mostly over  
15 central Europe while occasionally extending to southeast Europe [Emeis et al., 2011]. New  
16 significant eruptions occurred between May 4<sup>th</sup>–9<sup>th</sup> and May 14<sup>th</sup>–19<sup>th</sup> 2010 [Gudmundsson et  
17 al., 2010]. The first of these phases mainly influenced Western Europe, from Great Britain to  
18 the Iberian Peninsula, while the second phase influenced central Europe and the central and  
19 eastern Mediterranean on the May 18<sup>th</sup>–22<sup>nd</sup>. Final observations of the event were recorded  
20 over central Europe on the 25<sup>th</sup> of May [Gudmundsson et al., 2010]. Although the eruption  
21 was a moderate one, due to advection of the volcanic ash plumes, civil aviation was shut down  
22 for many days over numerous European countries [Gertisser., 2010]. This resulted in an  
23 urgent demand for reliable model forecasts of the vertical and horizontal extent of the ash  
24 plume, and for complementary measurements that could be used for nowcasting and forecast  
25 verification [Sears et al., 2013]. Following an eruption, Volcanic Ash Advisory Centres (VAAC)  
26 distributed around the globe give instructions to civil aviation in order avoid potential hazards  
27 [e.g. Guffanti et al., 2010]. Considering the large social and economic impact of any decision,  
28 the provided guidelines should be reliable, verifiable and should use all available scientific  
29 information [Zehner, 2010]. During the eruption period the European Aerosol Research Lidar  
30 Network, EARLINET, responded to this demand with coordinated intensive measurements  
31 from ground-based lidar [e.g. Ansmann et al, 2010; 2011; Groß et al., 2011; Mona et al., 2012;  
32 Papayannis et al., 2012; Perrone et al, 2012; Navas-Guzman et al, 2013; Pappalardo et al,  
33 2013]. This observation campaign provided information on ash height and its vertical extent,



1 as well as an estimation of the ash load in terms of optical depth and mass concentration. In  
2 addition, there were a number of dedicated airborne campaigns during the eruption that  
3 combined lidar and in-situ measurements of the ash plume [e.g. Marenco et al., 2011;  
4 Schumann et al, 2011]. The volcanic plume was observed from a variety of satellite sensors  
5 such as the Cloud-Aerosol Lidar with Orthogonal Polarization (CALIOP) on board the CALIPSO  
6 satellite [Winker et al., 2012] and a number of passive satellite sensors either in low Earth  
7 orbit, such as GOME-2/MetopA [e.g. Rix et al., 2012], MODIS/Terra & /Aqua [e.g. Christopher  
8 et al., 2012], IASI/MetopA [Carboni et al, 2012], or in geostationary orbit, such as SEVIRI [e.g.  
9 Francis et al., 2012]. The World Meteorological Organization organized an intercomparison  
10 campaign of twenty two satellite-based volcanic ash retrieval algorithms applied on passive  
11 sensors [WMO, 2015]. The intercomparison was based on six selected volcanic eruptions  
12 including Eyjafjallajökull. Validation results showed variable agreement with lidar data,  
13 depending upon the scene conditions.

14 In 2012 the European Space Agency (ESA) initiated the project “Satellite Monitoring of Ash  
15 and Sulphur Dioxide for the mitigation of Aviation Hazards” (SACS-2) to support authorities  
16 and the VAACs during future volcanic events. The project created an optimal end-to-end  
17 system for volcanic ash plume monitoring and prediction [Brenot et al., 2014 and  
18 <http://sacs.aeronomie.be>]. The system is based on improved and dedicated satellite-derived  
19 ash plume and sulphur dioxide products, followed by extensive validation using satellite and  
20 ground-based measurements [Koukouli et al., 2014a; Spinetti et al., 2014]. In this paper, we  
21 present validation results for two satellite sensors, GOME-2/MetOp-A and IASI/MetOp-A,  
22 concerning the volcanic ash optical depth and ash layer height, using ground and aircraft lidar  
23 measurements. The comparisons are restricted to the Eyjafjallajökull eruption period of 2010.  
24 In the first section we provide a short description of the satellite data and then a description  
25 of the ground-based and aircraft lidar data used as a reference for validation. Then we  
26 describe the methodology applied in the comparisons, and the co-location criteria applied. In  
27 the second section, we present the comparison results for the different sensors and  
28 algorithms, separately for the ground-based and aircraft data. Finally, we discuss the results  
29 and summarize our findings.

30

## 31 **2. DATA AND METHODOLOGY**

### 32 **2.1 SATELLITE DATA**



1 One of the main tasks of ESA's SACS-2 and SMASH (*Satellite Monitoring of Ash and Sulphur*  
2 *dioxide for the mitigation of aviation Hazards*) projects was to improve and validate the  
3 algorithms for the retrieval of ash optical depth and height, using satellite measurements in  
4 the infrared and UV-Vis from low Earth orbit sensors. These improvements were based on  
5 previous algorithm developments [e.g. de Graaf et al., 2005; Clerbaux et al., 2009; Clarisse et  
6 al, 2010, 2013; Gangale et al., 2010; Carboni et al., 2012; Grainger et al., 2013] In this paper  
7 we use data from GOME-2 and IASI instruments on board the MetOp-A satellite which covered  
8 the whole eruption period of Eyjafjallajökull in 2010. Details of the satellite data are described  
9 below.

#### 10 **2.1.1 GOME-2/METOP-A**

11 Data from GOME-2/MetOp-A have been processed by the Royal Netherlands Meteorological  
12 Institute (KNMI). The volcanic ash retrieval algorithm includes an estimation of the optical  
13 depth of an ash layer based on the Absorbing Aerosol Index (AAI) as well as an estimation of  
14 the effective ash layer height. The algorithm is based on look-up tables formed in terms of the  
15 absorbing aerosol index (AAI), aerosol height, solar zenith angle (SZA), view zenith angle (VZA),  
16 and relative azimuth angle (RAZI). The AAI is sensitive to atmospheric parameters such as  
17 aerosol type, aerosol layer height, and aerosol optical depth (AOD), and to surface height and  
18 scattering geometry [de Graaf et al., 2005]. The most dominant parameters are aerosol optical  
19 thickness and aerosol layer height. In general, thick aerosol layers produce larger AAI values  
20 than thin aerosol layers, while high altitude aerosol layers produce larger AAI values than low  
21 lying aerosol layers [Torres et al., 1998; de Graaf et al., 2005]. If the aerosol type, surface  
22 albedo, and geometries (SZA, VZA, RAZI) are known, aerosol optical thickness can be  
23 calculated using the AAI and aerosol height. The ash layer height is derived using the Fast  
24 REtrieval Scheme for Clouds from Oxygen A-band (FRESCO) algorithm [Wang et al., 2008a]. It  
25 has been demonstrated that FRESCO can retrieve volcanic ash layer height for optically thick  
26 ash plumes [Wang et al., 2012]. The retrieved optical thickness of the ash layer depends on  
27 the assumption of aerosol properties used in the look-up tables (LUTs). The volcanic ash  
28 particles are assumed to be spherical and have a bi-modal log-normal size distribution. Two  
29 different a priori assumptions for the refractive index of strongly absorbing volcanic ash were  
30 tested, indicated later on as DUST and VOLZ [Volz, 1973; Sinyuk et al., 2003.]

#### 31 **2.1.2 IASI/METOP-A**

32 Satellite estimates for the ash optical depth and layer height from IASI/Metop-A have been  
33 provided by two institutes, the Université Libre de Bruxelles (ULB) and the University of Oxford



1 (UOXF). The dataset provided by the ULB was generated by a LUT-based algorithm described  
2 in Moxnes et al. [2014] using two distinct sets of refractive indices: one set provided by Dr.  
3 Dan Peters [private communication] based on recent measurements of Eyjafjallajökull ash,  
4 and the other set using the basaltic ash refractive index data from Pollack et al, 1973 (referred  
5 to as the *Eyja* and *Pollack* datasets respectively). In this paper we show only estimates based  
6 on the *Eyja* refractive index. For this eruption, the ash plume was assumed to be centred at 5  
7 km and no attempt was made to retrieve ash plume height. The datasets provided by UOXF  
8 assume the *Eyja* refractive index, and both UOXF and ULB algorithms assume a log-normal  
9 particle size distribution with spread 2. The algorithmic processing of UOXF resulted in four  
10 different products: one characterized as the 'iterative' algorithm, which provided ash optical  
11 depth and layer height, and three characterized as the 'fast' algorithm, which provided ash  
12 optical depth for three fixed volcanic ash layer pressures (400 hPa, 600 hPa and 800 hPa). The  
13 fast algorithm, based on the method of Walker et al. [2011], carries out a linear retrieval (least  
14 squares fit) of the aerosol optical depth, AOD, assuming a fixed plume altitude and effective  
15 radius. The algorithm looks for departures in the measured spectra from an expected  
16 background covariance, created from previous IASI measurements containing no volcanic ash.  
17 The iterative algorithm is a full optimal estimation retrieval using a forward model based on  
18 Radiative Transfer for TOVS, *RTTOV*, a very fast radiative transfer model for nadir-viewing  
19 passive visible, infrared and microwave satellite radiometers. Clear sky radiances from *RTTOV*  
20 are combined with an ash layer in a method described in detail by Thomas et al. [2009a;  
21 2009b]. *RTTOV* then provides probable values of AOD, effective radius and plume altitude  
22 [Ventress et al. 2015]. The fast algorithm is used to flag IASI pixels (assuming an AOD threshold  
23 defined by the statistics of the scene) for the presence of volcanic ash, at which point the  
24 iterative retrieval is carried out on the pixel.

## 25 **2.2 LIDAR DATA**

26 The validation of the satellite products used lidar measurements from two sources. The first  
27 was the intensive ground-based lidar measurements from stations that form the European  
28 Research Lidar Network (EARLINET) and the second was the airborne lidar measurements  
29 from the UK's BAe-146-301 Atmospheric Research Aircraft managed by the Facility for  
30 Airborne Atmospheric Measurements (FAAM). The difference between the aircraft Lidar and  
31 the EARLINET stations in absolute AOD loadings may be significant, but is explainable. The  
32 aircraft flights monitored a large area affected by the ash cloud with high ash concentrations.  
33 Meanwhile, for most of the EARLINET stations, the volcanic particles atmospheric content was  
34 almost half of that observed in the UK, which was directly downwind from the eruption.



1 In the next section we provide a brief description of the lidar measurements used as reference  
2 data for the validation of the satellite products.

### 3 **2.2.1 EARLINET DATA**

4 Lidar data from the EARLINET network [Pappalardo et al., 2014 and <http://www.earlinet.org>]  
5 were used to validate ash plume height and optical depth. EARLINET was established in 2000  
6 and is the first aerosol lidar network with the main goal of providing data for investigating the  
7 aerosol distribution on a continental scale. EARLINET has established certain protocols for the  
8 measurements and the quality control of the systems and the retrieved data, through  
9 algorithm [Böckmann et al., 2004, Pappalardo et al., 2004] and system [Matthias et al., 2004a,  
10 Freudenthaler et al., 2010, Wandinger et al., 2015], intercomparison campaigns. The network  
11 currently includes 27 stations distributed over the European continent. The standard  
12 products of EARLINET include aerosol extinction and backscatter profiles. EARLINET data have  
13 been widely used for climatological studies [e.g. Matthias et al., 2004b; Amiridis et al., 2005;  
14 Giannakaki et al., 2007] as well as for monitoring unusual atmospheric events such as desert  
15 dust, biomass burning, pollution episodes, volcanic eruptions and so on. Results have been  
16 presented in numerous publications [e.g. Amiridis et al., 2009; Ansmann et al., 2003 ;  
17 Guerrero-Rascado et al., 2009; Mamouri et al., 2012; Mattis et al., 2010; Mona et al., 2006 ;  
18 Müller et al., 2007 ; Papayannis et al., 2008; Wang et al., 2008b].

19 A relational database, containing the output of the 4-D analysis of EARLINET data related to  
20 the volcanic eruption of 2010, has been set up [Mona et al., 2012; Pappalardo et al., 2013] and  
21 is freely available on request at <http://www.earlinet.org>. Information related to the present  
22 study involves aerosol backscatter coefficient profiles for each of the ground-based stations  
23 [The EARLINET publishing group 2000–2010, 2014], as well as a characterization of the  
24 observed layers as pure volcanic or mixed [Pappalardo et al., 2013]. A volcanic aerosol mask  
25 was developed [Mona et al., 2012], which involved aerosol typing, backward trajectory  
26 analyses and model outputs, used together with the lidar measurements at 1 hour temporal  
27 resolution. The data included in the EARLINET database captured the whole Eyjafjallajökull  
28 eruptive event over Europe providing geometrical and optical properties of the tropospheric  
29 volcanic cloud. The volcanic cloud persisted over central Europe for the whole period at  
30 heights of between 3 and 8 km, with maximum load observed on the 16<sup>th</sup> of April 2010 over  
31 Hamburg [Pappalardo et al., 2013]. In our study we only used profiles that corresponded to  
32 pure volcanic, as these were characterized by the methodology applied in Pappalardo et al.,



1 2013. The list of stations considered for the validation of the satellite products is shown in  
2 **Table I**.

### 3 **2.2.2 AIRCRAFT DATA**

4 The satellite products are validated using lidar measurements from six flights by the UK's BAe-  
5 146-301 Atmospheric Research Aircraft over the United Kingdom and the surrounding seas in  
6 May 2010 [e.g. Marengo et al., 2011; Johnson et al., 2011]. The lidar measurements include  
7 aerosol extinction profiles at 355 nm, which in turn provide plume height and layer optical  
8 depth. In situ observations were provided by other probes on the aircraft, in particular a  
9 three-wavelength nephelometer and PCASP and CAS optical particle counters; radiative  
10 measurements were taken in the visible and infrared. An example of the available aerosol  
11 extinction profiles, along with flight altitude and flight track is shown in **Figure 1** for the 16<sup>th</sup>  
12 of May 2010. The data shown here will be discussed in more detail in the overview of the  
13 comparison results. In this paper we mainly used lidar data from May 4<sup>th</sup>, 5<sup>th</sup>, 14<sup>th</sup>, 16<sup>th</sup>, 17<sup>th</sup>  
14 and 18<sup>th</sup> 2010 flights, when volcanic ash was detected and satellite data were available. Since  
15 the satellite AOD estimates were given at 550 nm we considered scaling the lidar-determined  
16 ash layer optical depth to 550 nm using an appropriate Angstrom exponent. According to  
17 Pappalardo et al. [2013] and based on EARLINET observations, the Angstrom exponent  
18 between 355 and 532 nm ranges between 0.03 and -0.11. So we used an exponent equal to  
19 zero, which practically means that the optical depths to be compared were not scaled.

20

#### 21 **2.2.2.1 METHODOLOGY FOR THE EARLINET-SATELLITE COMPARISONS**

22 The values of each satellite product have been restricted to an area of variable radius around  
23 each EARLINET station, depending on the satellite. The closest point in space and time has  
24 been selected for each overpass, and compared to the respective layer characterized by  
25 EARLINET as volcanic particles. Spatial filtering is applied before the temporal filtering. The  
26 EARLINET relational database for this event contains cases for which two or more volcanic  
27 layers are simultaneously observed in the atmospheric column. For these cases the worst  
28 correlated layer to the satellite data was excluded from analysis. A summary of the satellite  
29 data compared with the EARLINET measurements and the corresponding collocation criteria  
30 can be found in **Table II**. For all the satellite products a comparison of the AOD has taken  
31 place. For the satellite products that provided volcanic ash layer height information a  
32 comparison of volcanic ash layer height was also performed. The AOD of the EARLINET layers  
33 was derived by the layers' integrated backscatter coefficient multiplied by a fixed extinction-



1 to-backscatter ratio with a value of  $50 \text{ sr}^{-1}$  [Ansmann et al., 2010]. We did not use any Raman  
2 lidar measurements since most comparisons were performed for daytime conditions. An  
3 estimated 20% uncertainty on the EARLINET AOD was applied due to the variability of the lidar  
4 ratio for volcanic particles, typically between 40 and  $60 \text{ sr}^{-1}$  [see Pappalardo et al., 2013 and  
5 references therein]. For the layer height comparison, the height of the centre of mass  
6 provided by the EARLINET database was used, and as estimated layer depth, the distance  
7 between the mass centre from the layer top and base was employed. All the satellite ash  
8 optical depth products were calculated at 550 nm, apart from the KNMI/GOME2 products  
9 which were calculated first at 380 nm and then scaled to 550 nm using appropriate Angstrom  
10 exponents provided by the satellite team. In order to convert the infrared optical depth to  
11 optical depth at 550 nm, both ULB and UOXF teams used the Eyja refractive indices from Dr.  
12 Dan Peters (private communication). Correspondingly, 532 nm lidar measurements were used  
13 in the comparisons.

#### 14 2.2.2.2 METHODOLOGY FOR THE AIRCRAFT-SATELLITE COMPARISONS

15 The airborne lidar data were available on a per flight basis [Koukouli et al., 2014b] and  
16 included aerosol extinction profiles that provided ash plume height and ash layer optical  
17 depth. The values of these variables were compared with the satellite produced values of ash  
18 optical depth and aerosol layer height (where given) over an area of variable radius ranging  
19 from 50 km to 200 km. The closest satellite value in terms of spatial proximity for every flight  
20 path location was found and presented. Since the overpass times of the satellite data are  
21 around 9:30 L.T. and 21:30 L.T., in order to allow for co-location, only spatial criteria were  
22 used. None of the available aircraft data were available within 1-2 hours of the overpass time,  
23 which was the criterion that provided the best matches when using the EARLINET data. The  
24 time difference between satellite and aircraft data was around 5 hours. This fact does not  
25 allow a point-to-point comparison of the measurements but the comparisons will mainly  
26 highlight whether the ash products from the two measuring systems are consistent. A  
27 summary of the satellite data compared against the flight measurements and the  
28 corresponding collocation criteria can be found in **Table III**.

29

### 30 3. RESULTS AND DISCUSSION

#### 31 3.1 COMPARISON OF ASH OPTICAL DEPTH AND ASH LAYER HEIGHT 32 WITH EARLINET DATA





1 As shown in **Table III**, we applied different collocation criteria between the EARLINET lidar  
2 measurements and the satellite observations, to investigate which one provides the best  
3 results and a reasonable number of matches. Although during April and May 2010 the  
4 EARLINET stations performed a large number of dedicated intensive measurements, the  
5 overpass time of the MetOP-A satellite significantly limited the number of collocations. We  
6 examined, for each of the collocation criteria, the correlation coefficient between the lidar-  
7 determined optical depth of the pure volcanic particles layer and the corresponding satellite  
8 estimate. Furthermore, we examined the correlation coefficient between the ash layer height  
9 estimated from the lidar measurements and the one retrieved from the satellite algorithms  
10 when available [Koukouli et al., 2014b]. In Figure 2 we present scatter plots between EARLINET  
11 ash layer optical depth and each satellite ash product for those collocation criteria that  
12 showed the largest correlation. The best correlations were found when limiting the matches  
13 to within a radius of 100 km from the ground-based lidar and considering measurements with  
14 a one-hour difference. When deviating from these criteria, the number of matches increased  
15 but the correlation declined. This fact provides an indication of the spatial and temporal  
16 representativeness of single lidar profiles. Different colours in these plots correspond to  
17 different European regions (see **Table I**) in order to examine whether the distance from the  
18 source and the transport path have an impact on the comparisons.

19 The GOME-2A comparisons are shown in the Figure 2a and 2b with the “dust” algorithm in  
20 the left column and the “Volz” algorithm in the right column. Only twelve collocations were  
21 found for the GOME-2 and the EARLINET observations. There is a small correlation between  
22 the datasets, ranging between 0.33 and 0.46 for the “dust” and “Volz” products respectively.  
23 This limited number of co-locations were given by a radius of 300 km from each ground-based  
24 station and within 5 hours. The GOME-2A estimates of the ash layer optical depth are  
25 systematically larger than the lidar ones and most of them are larger than 1, although for  
26 these cases the lidar data rarely exceed the value 0.5. The large GOME-2 pixel size (80 km x  
27 40 km) and the large search radius (300 km) could partly explain differences with point  
28 measurements, like the lidar; however it seems possible that many GOME-2A data are  
29 contaminated by thin clouds, while the lidar data included in the EARLINET database are  
30 always cloud screened. Between the two GOME-2A products the “Volz” algorithm shows a  
31 slightly better correlation coefficient with the ground-based lidars.

32 The scatter plots of UOXF ash optical depth and collocated EARLINET measurements are  
33 presented in Figure 2c and 2d; the plot in the left column corresponds to the iterative



1 algorithm and the right column corresponds to the “fast” algorithm at a fixed height of 600  
2 hPa, which is consistent with the average height where EARLINET observed volcanic particles.  
3 For both algorithms the collocation criteria that provided the best results were a distance from  
4 each ground-based station of 100 km and a maximum time difference of one hour. These  
5 criteria allowed for almost 20 coincidences. As it can be quickly verified by the results shown  
6 in Figure 2c and 2d, the ash AOD extracted from the IASI/MetOpA Oxford iterative algorithm  
7 is quite low, with values rarely rising above 0.2, which is consistent with the EARLINET  
8 measurements, which show similar AOD levels. There are only two cases showing AOD values  
9 larger than 0.2 and these are also consistent with EARLINET, since the lidar data for these two  
10 cases show significantly larger values, above 0.4. The correlation coefficient is quite promising  
11 at 0.85, however it is based on only 18 coincident measurements. The agreement between  
12 IASI and EARLINET estimates is similar for the “fast” algorithm, showing a larger scatter for  
13 the low AOD values but potentially less scatter for larger AODs. This larger scatter leads to a  
14 smaller correlation coefficient close to 0.78. If we loosen the collocation criteria to 300 km  
15 and 3 hours then the correlation coefficient drops significantly to a value of less than 0.5.

16 In Figure 2e we show comparisons of the ash optical depth from the ULB algorithm with  
17 EARLINET estimates. The results are shown for the same collocation criteria applied to UOXF  
18 comparisons, i.e. 100 km distance and one hour difference between the observations. The  
19 general picture is consistent with the IASI/UOXF datasets, however the number of  
20 coincidences decreases. The comparisons show a correlation of 0.91, which is the largest  
21 found in all comparisons shown in Figure 2. **Table IV** provides the mean EARLINET and satellite  
22 ash optical depths for the coincidences shown in Figure 2. The average AOD values of the  
23 measurements that meet the collocation criteria are small (less than 0.2) and consistent with  
24 each other, except in the case of GOME-2A and when the IASI-UOXF fast algorithm has a fixed  
25 height of 800 hPa, where the satellite data overestimate the ash optical depth. We have to  
26 repeat that the mean values are based on a small number of coincidences.

27 The GOME-2A ash products and the iterative IASI product processed by UOXF provided the  
28 height of the ash layer. These heights were compared with the estimates from EARLINET and  
29 the results are shown in **Figure 3**. The ash plume height estimated for GOME-2A products and  
30 the EARLINET network are compared in Figure 3a. Irrespective of the product and the search  
31 radius (not shown here) the comparison is not satisfactory for either of the two algorithms.  
32 The satellite-provided height seems to strongly under-estimate the ground-based values,  
33 showing a very narrow range of values between 1 and 2 km. The ground instruments show a



1 more physical spread of the ash cloud locating it between 3 and 6 km. The comparison of the  
2 ash plume height extracted from the IASI/MetopA UOXF iterative algorithm and the one  
3 observed by the EARLINET network is shown in **Figure 3b**. It is evident from this figure that  
4 the spread of plume heights found by the EARLINET network is higher than those found by the  
5 Oxford iterative IASI algorithm leading to rather poor correlations. The estimate of the mean  
6 is consistent between the datasets. This fact is demonstrated in the summary **Table V** which  
7 gives the mean EARLINET and satellite ash plume height estimates. The large scatter bars  
8 indicate the variability inherent in both sets of observations. We have to note here that the  
9 UOXF-fast algorithm with fixed heights for the ash performs better for 600 hPa, which is  
10 consistent with the average heights estimated by the nominal algorithm and the EARLINET  
11 data, which range between 3 and 4 km. In all lidar-satellite comparisons there was no  
12 indication that there were regions where the agreement between the two datasets is better,  
13 due to their proximity to the source. However this conclusion is based, especially for certain  
14 regions, on extremely few data.

15

### 16 **3.2 COMPARISONS OF ASH OPTICAL DEPTH AND ASH LAYER** 17 **HEIGHT WITH AIRBORNE LIDAR DATA**

18 During May 2010 there were 12 flights of the UK's BAe-146-301 Atmospheric Research Aircraft  
19 [Marenco et al., 2011], and during six of these volcanic ash was detected in the airborne lidar  
20 measurements. In order to avoid contamination from cirrus clouds and mixed aerosol layers,  
21 we only show comparisons with the satellite data for two flights, during which significant  
22 levels of pure ash, not mixed with other aerosol types, were observed by the airborne lidar  
23 measurements. The flight that took place on the 16<sup>th</sup> of May 2010 (see also Figure 1), started  
24 at 12:55 U.T. and ended at 18:00 U.T. and the aircraft mostly flew over Scotland and northern  
25 England. During this flight most of the ash was observed between 55° and 56°N. The flight  
26 that took place on the 17<sup>th</sup> of May over the Irish and North Sea, started a little earlier at 11:15  
27 U.T. and ended at 16:58 U.T., and most of the ash was observed over the North Sea between  
28 1° and 2°E. As is demonstrated in **Table III**, we only used spatial criteria to find coincidences  
29 between the airborne lidar data and the satellite data of the same day, since both flights were  
30 performed in the afternoon, while the satellite overpasses are close to 9:30 U.T. (GOME-2A  
31 and IASI) and 21:30 U.T. (IASI only). For GOME-2 we found coincidences only for the 17<sup>th</sup> of  
32 May 2010.



1 In **Figure 4** we show the comparisons of the satellite ash optical depth and the airborne lidar  
2 ash layer optical depth for 550 nm as a function of aircraft time (closest point in space). We  
3 also show in the bottom row of **Figure 4** (4e and 4f) the flight track for the two flights  
4 examined. On the path the actual flight time is indicated, in order to be able to identify the  
5 spatial location that corresponds to the footprint of the lidar data. Since the time difference  
6 between the flight measurement and the satellite overpass is large what we would actually  
7 see from the comparisons is (a) if the aircraft and the satellite observe the plume over the  
8 same area and (b) if they observe similar optical depth values. This would occur if the  
9 dispersion, or transport, of the plume was not significant during the hours elapsing between  
10 the satellite overpass and the aircraft measurement, within the spatial criteria we applied for  
11 the comparisons. In the **Figure 4a** and **4b** we show the comparisons between IASI ash optical  
12 depth for the iterative and fast algorithm of UOXF versus the ash layer optical depth from the  
13 airborne lidar measurements for the 16<sup>th</sup> of May 2010, where the measurements are shown  
14 as function of time in U.T.C. In **Figure 4e** and **4f**, we plot the flight path for the two days (16  
15 and 17 May 2010). Along the path the flight time in U.T.C is posted, while the different colours  
16 along the flight path indicate the ash optical depth. As we can see, the satellite data processed  
17 with the iterative UOXF algorithm captures the high AODs observed around 14:00 U.T. and  
18 between 16:00 and 17:00 U.T. quite well, but fails to capture the peak observed between  
19 15:00 and 16:00 U.T. In addition, it seems that the background is similar but that some larger  
20 values are observed between the ash peaks. The situation is slightly different when examining  
21 the comparisons between the aircraft data and the estimates from the UOXF fast algorithm  
22 using a fixed height of the ash layer at 600 hPa. In general, the UOXF fast algorithm estimates  
23 smaller values (including the background); it captures well the peak observed around 14:00  
24 U.T., overestimates the peak in AOD observed between 15:00 and 16:00 U.T. and it is hard to  
25 tell if the smaller peak observed around 17:00 U.T. is well-depicted or not.

26 In **Figure 4c**, we present the comparisons between the aircraft data and the estimates from  
27 the ULB-Eyja algorithm again for the 16<sup>th</sup> of May 2010. The satellite estimates follow quite  
28 well all peaks observed in the aircraft data, however slightly misplaced. Checking the SEVIRI  
29 ash imagery at <http://fred.nilu.no> for the 16<sup>th</sup> of May 2010 we observe an almost constant  
30 west-east flow of dust throughout the day between 55°N and 58° N, and thus this plume was  
31 captured both by the morning and by the evening orbit of IASI, as well as by the aircraft when  
32 flying over these latitudes between 14:00 and 16:00 UT. SEVIRI observed a plume after 17:00  
33 UT south of 54° N moving southeast. The early evolution of this plume was captured by the  
34 aircraft around 17:00 and its later evolution was captured over the same area by the evening



1 orbit of IASI. This plume evolution can partly explain the displacement observed, since the  
2 satellite data are not coincident in time with the aircraft data and the time in x-axis of the  
3 plots actually corresponds to different latitude/longitude of the comparisons.

4 In **Figure 4d** we present the corresponding comparisons between the aircraft data and the  
5 estimates from the GOME-2 KNMI algorithm for the 17<sup>th</sup> of May 2010, and in the right hand  
6 column of the last row of Figure 4 the corresponding flight path of the aircraft. The GOME-2  
7 results capture the levels of the two AOD peaks observed in the aircraft measurements but  
8 fail to capture small scale variability in the AOD and the background levels. In these cases we  
9 actually compare only the morning orbit (9:30 UT) since GOME-2 is a UV/Vis sensor. SEVIRI  
10 images show a southeast movement of the ash plume starting east of the coast of England  
11 and going towards the Netherlands. The east-west motion of the aircraft over the sea  
12 captured this plume between 14:30 and 15:00, and GOME-2 observed this plume over the  
13 same area in the morning. Before 14:30 UT the aircraft was flying over land and did not  
14 observe any significant ash, so when compared with the morning observations of GOME-2 and  
15 considering the pixel size of GOME-2 and the collocation criteria applied, these measurements  
16 are actually compared with satellite data over the sea. Considering the large time difference  
17 between the flight and GOME-2 overpass and the much larger pixel size of GOME-2, compared  
18 to IASI, it is remarkable that the satellite data can quantitatively capture the ash optical depth  
19 in the greater flight area. **Table VI** summarizes the mean AODs values observed from the  
20 aircraft lidar and each of the satellite products examined.

21 Finally, in **Figure 5** we present the comparisons of the ash layer height observed from the  
22 aircraft measurements and the corresponding effective ash height estimated from the UOXF-  
23 iterative algorithm based on IASI (Figure 5a) and the KNMI algorithm based on GOME-2 (Figure  
24 5b). Considering the constraints induced by the collocation criteria, both algorithms show very  
25 good agreement with the corresponding heights estimated from the airborne lidar data in  
26 most of the collocations, with the ash height mainly ranging between 3 and 5 km. **Table VII**  
27 summarizes the mean ash layer height observed from the aircraft measurements and each  
28 satellite product examined.

#### 29 **4. SUMMARY AND CONCLUSIONS**

30 The main aim of this work is to present the validation of improved and dedicated satellite-  
31 derived ash plume level assessments as part of the European Space Agency initiatives, in order  
32 to create an optimal “*End-to-End System for Volcanic Ash Plume Monitoring and Prediction*  
33 systems”. The results shown are complementary to other satellite volcanic ash products, e.g.



1 from SEVIRI (Prata and Prata, 2012, Clarisse and Prata, 2015, WMO, 2015). Different aerosol  
2 optical depth and ash plume height estimations from GOME2/MetopA and IASI/MetopA have  
3 been assessed against collocated ground-based and airborne Lidar data for the 2010 eruptions  
4 of the Icelandic volcano Eyjafjallajökull. The GOME2/MetopA measurements have been  
5 analysed by the Royal Netherlands Meteorological Institute (KNMI) and the IASI/MetopA  
6 observations by both the Université Libre de Bruxelles (ULB) and the University of Oxford  
7 (UOXF). Different algorithm versions and parameters were examined and inter-compared.  
8 Both aerosol optical depth and ash plume height satellite estimates were compared with  
9 European Aerosol Research Lidar Network [EARLINET] lidar measurements and the UK's BAe-  
10 146-301 Atmospheric Research Aircraft flying over the UK during the eruptive period.

- 11 ▪ The KNMI GOME2 AOD over-estimates the ground-based values, showing quite high  
12 values for cases where the LIDAR sees a low AOD. As a result, the *dust* algorithm shows  
13 relatively low correlation coefficients of between 0.25 and 0.3 depending on the  
14 spatiotemporal search radius, whereas the *Volz* algorithms perform slightly better, with  
15  $r^2$  values ranging between 0.4 and 0.5. The KNMI/GOME2 data seem to suffer from the  
16 spatial resolution of the satellite instrument which made the spatial criterion rather too  
17 large hence precluding any conclusive comparisons when compared to the aircraft  
18 measurements. The agreement between the satellite-derived and airborne lidar effective  
19 ash heights differ only by 1 km on the average, indicating a homogenous spread of the  
20 plume under the satellite's pixel. The KNMI GOME2 ash plume height comparisons are  
21 not satisfactory, irrespective of the search radius, for either of the two algorithms. The  
22 satellite ash height values seem to under-estimate the ground-based values, having a very  
23 narrow range of values between 1 and 2 km and a mean of  $2.07 \pm 1.22$  km. In comparisons,  
24 the ground instruments show a more natural spread between 3 and 6 km with a mean of  
25  $3.92 \pm 1.22$  km. It is highly likely that the large GOME-2 pixel size smooths out any small  
26 scale variability of the plume height, otherwise captured by the ground-based single point  
27 measurements.
- 28 ▪ The Oxford nominal IASI algorithm shows satisfactory AOD correlations against the  
29 ground AODs, with coefficients ranging between 0.6 and 0.85, and, even though it  
30 provides rather small optical depths, these are of the same order of magnitude as the  
31 lidar. The algorithm presents quite good comparisons for the AOD patterns observed with  
32 aircraft lidar. The Oxford nominal IASI algorithm ash plume height comparisons do not  
33 show any significant correlation with the EARLINET estimates. The satellite estimates have  
34 no spread in values compared to the lidar estimates, however both datasets show similar



1 average values, indicating that the satellite estimates can capture the average conditions.  
2 The results are better when compared with the aircraft lidar, where it seems that the  
3 satellite estimates follow the variability of ash height along the flight route; however they  
4 slightly underestimate the height values with a mean of  $3.73 \pm 1.45$  km [compared to the  
5 aircraft mean of  $4.30 \pm 2.00$  km].

- 6 ■ The Oxford fast IASI algorithm also provides the same order of magnitude AOD estimates  
7 as the ground lidar, with the narrower spatio-temporal choice providing the most  
8 promising results: the 400 hPa product has a correlation of around 0.7 and the 800 hPa  
9 product a correlation of around 0.8. The Oxford fast IASI algorithm shows an excellent  
10 agreement with the aircraft lidar, where the 600 hPa product, that corresponds to the  
11 actual plume height, appears to perform best.
- 12 ■ The ULB AOD estimates are the most promising, showing the highest correlation  
13 coefficients, ranging between 0.74 and 0.91, depending on the spatio-temporal criterion  
14 chosen. This is also valid when we examine the ULB IASI – aircraft comparisons. The ULB  
15 IASI algorithm shows excellent agreement, both with respect to the absolute AOD values  
16 and with AOD features during the flight shown. The actual absolute AOD maxima are also  
17 represented best by this product.

18

19 Concluding, we note that, depending on the careful choice of collocation criteria, the satellite  
20 algorithms investigated here can observe the ash optical depth and plume height for large  
21 enough eruptions to a satisfactory degree. The results shown in this study are in line with the  
22 main finding of the dedicated WMO intercomparison study [2015] concerning the agreement  
23 between satellite ash products and validation data sets (for AOD correlations between 0.4 and  
24 0.6 and ash layer height agreement within 2 km) and in some cases the results shown here  
25 show better statistics. However, in order to quantify the levels of accuracy of the satellite  
26 assessments, eruptions with strong ash plumes need to be included in this type of validation  
27 exercise, since there were too few co-location scenes for most satellite products for the  
28 Eyjafjallajökull and Grimsvötn 2010 and 2011 eruptions, as examined in the course of the  
29 SACS/SMASH ESA projects. This validation study highlights the need for dedicated validation  
30 campaigns during volcanic eruptions. For future eruptions it could be recommended to fly  
31 instrumented aircraft along the satellite orbit in order to optimize the collocations between  
32 satellite data and aircraft-based observations. It is recognised that this would be a difficult  
33 campaign to plan, given that it is not possible to make precise long-term predictions of the  
34 eruptions.



1

## 2 **Acknowledgements**

3 The comparison study was funded by the European Space Agency in the frame of the “Satellite  
4 Monitoring of Ash and Sulphur dioxide for the mitigation of Aviation Hazards”-SACS-2 project.  
5 The financial support for EARLINET in the ACTRIS Research Infrastructure Project by the  
6 European Union’s Horizon 2020 research and innovation program under grant agreement n.  
7 654169 and previously under grant agreement n. 262254 in the 7thFramework Program  
8 (FP7/2007-2013) is gratefully acknowledged. The UK’s BAe-146-301 Atmospheric Research  
9 Aircraft flown by Directflight Ltd and managed by the Facility for Airborne Atmospheric  
10 Measurements (FAAM), which a joint entity of the Natural Environment Research Council  
11 (NERC) and the Met Office. L.C. is a research associate with the Belgian F.R.S.-FNRS. LJV was  
12 funded through the NERC National Centre for Earth Observation. RGG and EC were supported  
13 by the NERC Centre for Observation and Modelling of Earthquakes, Volcanoes, and Tectonics  
14 (COMET).

15

16

17





## 1 References

- 2 Ansmann, A., et al., (2003), Long-range transport of Saharan dust to northern Europe: The 11-  
3 16 October 2001 outbreak with EARLINET, *Journal of Geophysical Research*, 108, 4783, doi:  
4 10.1029/2003JD003757.
- 5 Ansmann, A., et al. (2010), The 16 April 2010 major volcanic ash plume over central Europe:  
6 EARLINET lidar and AERONET photometer observations at Leipzig and Munich, Germany,  
7 *Geophys. Res. Lett.*, 37, L13810, doi:10.1029/2010GL043809.
- 8 Ansmann, A., et al. (2011), Ash and fine-mode particle mass profiles from EARLINET-AERONET  
9 observations over central Europe after the eruptions of the Eyjafjallajökull volcano in 2010,  
10 *J. Geophys. Res.*, 116, D00U02, doi:10.1029/2010JD015567.
- 11 Amiridis V., D. Balis, S. Kazadzis, A. Bais, E. Giannakaki, A. Papayannis and C. Zerefos, (2005),  
12 Four years aerosol observations with a Raman lidar at Thessaloniki, Greece in the  
13 framework of EARLINET, *J. Geophys. Res.*, Vol. 110, D21203, doi:10.1029/2005JD006190.
- 14 Amiridis, V., Balis, D. S., Giannakaki, E., Stohl, A., Kazadzis, S., Koukouli, M. E., and Zanis, P.,  
15 (2009), Optical characteristics of biomass burning aerosols over Southeastern Europe  
16 determined from UV-Raman lidar measurements, *Atmos. Chem. Phys.*, 9, 2431-2440,  
17 doi:10.5194/acp-9-2431-2009.
- 18 Brenot, H., et al., (2014), Support to Aviation Control Service (SACS): an online service for near-  
19 real-time satellite monitoring of volcanic plumes, *Nat. Hazards Earth Syst. Sci.*, 14, 1099-  
20 1123, doi:10.5194/nhess-14-1099-2014.
- 21 Böckmann, C., U. Wandinger, A. Ansmann, et al., (2004), Aerosol lidar intercomparison in the  
22 framework of EARLINET: Part II-Aerosol backscatter algorithms, *Applied Optics* 43, 977-  
23 989.
- 24 Carboni, E., Grainger, R., Walker, J., Dudhia, A., and Siddans, R. (2012), A new scheme for  
25 sulphur dioxide retrieval from IASI measurements: application to the Eyjafjallajökull  
26 eruption of April and May 2010, *Atmos. Chem. Phys.*, 12, 11417-11434, doi:10.5194/acp-  
27 12-11417-2012.
- 28 Christopher, S. A., N. Feng, A. Naeger, B. Johnson, and F. Marengo (2012), Satellite remote  
29 sensing analysis of the 2010 Eyjafjallajökull volcanic ash cloud over the North Sea during  
30 4–18 May 2010, *J. Geophys. Res.*, 117, D00U20, doi:10.1029/2011JD016850.
- 31 Clarisse, L., Hurtmans, D., Prata, A. J., Karagulian, F., Clerbaux, C., Mazière, M. D. and Coheur,  
32 P.-F., (2010), Retrieving radius, concentration, optical depth, and mass of different types  
33 of aerosols from high-resolution infrared nadir spectra, *Appl. Opt.*, 49, 3713-3722, doi:  
34 10.1364/AO.49.003713.
- 35 Clarisse, L., Coheur, P.-F., Prata, F., et al., (2013), A unified approach to infrared aerosol  
36 remote sensing and type specification, *Atmos. Chem. Phys.*, 13, 2195-2221,  
37 doi:10.5194/acp-13-2195-2013.
- 38 Clarisse, L and F. Prata (2015), Infrared sounding of volcanic ash, in *Volcanic Ash: Methods of  
39 observation and monitoring* (eds S. Mackie, K. Cashman, A. Rust, H. Ricketts and I.M.  
40 Watson), in press
- 41 Clerbaux, C., Boynard, A., Clarisse, L., et al., (2009), Monitoring of atmospheric composition  
42 using the thermal infrared IASI/MetOp sounder, *Atmos. Chem. Phys.*, 9, 6041-6054,  
43 doi:10.5194/acp-9-6041-2009.



- 1 The EARLINET publishing group 2000-2010, Adam, M., Alados-Arboledas, L., Althausen, D.,  
2 Amiridis, V., Amodeo, A., Ansmann, A., Apituley, A., Arshinov, Y., Balis, D., Belegante,  
3 L., Bobrovnikov, S., Boselli, A., Bravo-Aranda, J. A., Bösenberg, J., Carstea, E., Chaikovsky, A.,  
4 Comerón, A., D'Amico, G., Daou, D., Dreischuh, T., Engelmann, R., Finger, F.,  
5 Freudenthaler, V., Garcia-Vizcaino, D., García, A. J. F., Geiß, A., Giannakaki, E., Giehl, H.,  
6 Giunta, A., de Graaf, M., Granados-Muñoz, M. J., Grein, M., Grigorov, I., Groß, S., Gruening,  
7 C., Guerrero-Rascado, J. L., Haeffelin, M., Hayek, T., Iarlori, M., Kanitz, T., Kokkalis, P., Linné,  
8 H., Madonna, F., Mamouri, R.-E., Matthias, V., Mattis, I., Menéndez, F. M., Mitev,  
9 V., Mona, L., Morille, Y., Muñoz, C., Müller, A., Müller, D., Navas-Guzmán, F., Nemuc, A.,  
10 Nicolae, D., Pandolfi, M., Papayannis, A., Pappalardo, G., Pelon, J., Perrone, M. R.,  
11 Pietruczuk, A., Pisani, G., Potma, C., Preißler, J., Pujadas, M., Putaud, J., Radu, C., Ravetta,  
12 F., Reigert, A., Rizi, V., Rocadenbosch, F., Rodríguez, A., Sauvage, L., Schmidt, J., Schnell, F.,  
13 Schwarz, A., Seifert, P., Serikov, I., Sicard, M., Silva, A. M., Simeonov, V., Siomos, N., Sirch,  
14 T., Spinelli, N., Stoyanov, D., Talianu, C., Tesche, M., De Tomasi, F., Trickl, T., Vaughan, G.,  
15 Volten, H., Wagner, F., Wandinger, U., Wang, X., Wiegner, M., and Wilson, K. M.: EARLINET  
16 observations related to volcanic eruptions (2000–2010), World Data Center for Climate  
17 (WDCC), doi:10.1594/WDCC/EN\_VolcanicEruption\_2000-2010, 2014.
- 18
- 19 Giannakaki, E., Balis, D. S., Amiridis, V., and Kazadzis, S., (2007), Optical and geometrical  
20 characteristics of cirrus clouds over a Southern European lidar station, Atmos. Chem. Phys.,  
21 7, 5519-5530, doi:10.5194/acp-7-5519-2007.
- 22 de Graaf, M., P. Stammes, O. Torres, and R. B. A. Koelemeijer (2005), Absorbing Aerosol Index:  
23 Sensitivity analysis, application to GOME and comparison with TOMS, J. Geophys. Res.,  
24 110, D01201, doi:10.1029/2004JD005178.
- 25 Gertisser R., (2010), Eyjafjallajökull causes widespread disruption to European air traffic, Geol.  
26 Today, 26, 94-95
- 27 Groß, S., V. Freudenthaler, M. Wiegner, J. Gasteiger, A. Geiß, and F. Schnell (2011), Dual-  
28 wavelength linear depolarization ratio of volcanic aerosols: lidar measurements of the  
29 Eyjafjallajökull plume over Maisach, Germany, Atmos. Environ., 48, 85-96, doi:  
30 10.1016/j.atmosenv.2011.06.017.
- 31 Gudmundsson, M. T., R. Pedersen, K. Vogfjörð, B. Thorbjarnardóttir, S. Jakobsdóttir, and M. J.  
32 Roberts (2010), Eruptions of Eyjafjallajökull Volcano, Iceland, Eos Trans. AGU, 91(21), 190-  
33 191, doi:10.1029/2010EO210002.
- 34 Guerrero-Rascado, J. L., Olmo, F. J., Avilés-Rodríguez, I., Navas-Guzmán, F., Pérez-Ramírez, D.,  
35 Lyamani, H., and Alados Arboledas, L., (2009), Extreme Saharan dust event over the  
36 southern Iberian Peninsula in September 2007: active and passive remote sensing from  
37 surface and satellite, Atmos. Chem. Phys., 9, 8453-8469, doi:10.5194/acp-9-8453-2009.
- 38 Guffanti M., D.J. Schneider, K.L. Wallace, T. Hall, D.R. Bensimon and L.J. Salinas (2010),  
39 Aviation response to widely dispersed volcanic ash and gas cloud from the August 2008  
40 eruption of Kasatochi, Alaska, USA, J. Geophys. Res., 115, D00L19,  
41 doi:10.1029/2010JD013868.
- 42 Johnson, B., et al. (2012), In situ observations of volcanic ash clouds from the FAAM aircraft  
43 during the eruption of Eyjafjallajökull in 2010, J. Geophys. Res., 117, D00U24,  
44 doi:10.1029/2011JD016760
- 45 Emeis, S., Forkel, R., Junkermann, W., Schäfer, K., Flentje, H., Gilge, S., Fricke, W.,  
46 Wiegner, M., Freudenthaler, V., Groß, S., Ries, L., Meinhardt, F., Birmili, W., Münkel, C.,  
47 Obleitner, F., and Suppan, P.: Measurement and simulation of the 16/17 April 2010



- 1 Eyjafjallajökull volcanic ash layer dispersion in the northern Alpine region, *Atmos. Chem.*  
2 *Phys.*, 11, 2689-2701, doi:10.5194/acp-11-2689-2011, 2011.
- 3 Francis, P. N., M. C. Cooke, and R. W. Saunders (2012), Retrieval of physical properties of  
4 volcanic ash using Meteosat: A case study from the 2010 Eyjafjallajökull eruption, *J.*  
5 *Geophys. Res.*, 117, D00U09, doi:10.1029/2011JD016788.
- 6 Freudenthaler, V., et al., (2010), EARLI09 – direct intercomparison of eleven EARLINET lidar  
7 systems, in: Proceedings of the 25th International Laser Radar Conference, St. Petersburg,  
8 Russia, 5–9 July, 891–894.
- 9 Koukouli, M. E., L. Clarisse, E. Carboni, et al., (2014a), Intercomparison of Metop-A SO<sub>2</sub>  
10 measurements during the 2010-2011 Icelandic eruptions, *Annals in Geophysics*, Vol 57,  
11 Fast Track 2, <http://dx.doi.org/10.4401/ag-6613>.
- 12 Koukouli, M. E., et al. (2014b), SACS2/SMASH Validation Report on the Eyjafjallajökull &  
13 Grímsvötn Eruptions, [http://sacs.aeronomie.be/Documentation/LAP-AU.T.H-SACS-](http://sacs.aeronomie.be/Documentation/LAP-AU.T.H-SACS-ValidationReport_FINAL.pdf)  
14 [ValidationReport\\_FINAL.pdf](http://sacs.aeronomie.be/Documentation/LAP-AU.T.H-SACS-ValidationReport_FINAL.pdf), last accessed: Tuesday, January 19, 2016.
- 15 Levelt P.F., et al., (2006), The Ozone Monitoring Instrument, *IEEE Trans. Geosc. Rem. Sens.*, 44  
16 (5), 1093-1101.
- 17 Gangale, G., A. J. Prata, and L. Clarisse (2010), The infrared spectral signature of volcanic ash  
18 determined from high spectral resolution satellite measurements, *Remote Sens.*  
19 *Environ.*, 114, 414–425, [10.1016/j.rse.2009.09.007](http://dx.doi.org/10.1016/j.rse.2009.09.007).
- 20 Grainger, R. G., D. M. Peters, G. E. Thomas, A. Smith, R. Siddans, E. Carboni, and A. Dudhia  
21 (2013), Measuring volcanic plume and ash properties from space, in remote sensing of  
22 volcanoes and volcanic processes: Integrating observation and modelling, *Geol. Soc. Spec.*  
23 *Publ.*, 380, doi:10.1144/SP380.7.
- 24 Mamouri, R. E., Papayannis, A., Amiridis, V., Müller, D., Kokkalis, P., Rapsomanikis, S.,  
25 Karageorgos, E. T., Tsaknakis, G., Nenes, A., Kazadzis, S., and Remoundaki, E., (2012), Multi-  
26 wavelength Raman lidar, sun photometric and aircraft measurements in combination with  
27 inversion models for the estimation of the aerosol optical and physico-chemical properties  
28 over Athens, Greece, *Atmos. Meas. Tech.*, 5, 1793-1808, doi:10.5194/amt-5-1793-2012.
- 29 Matthias V., J. Bösenberg, V. Freudenthaler, A. Amodeo, D. Balis, A. Chaikovsky, G. Chourdakis,  
30 A. Comeron, A. Delaval, F. de Tomasi, R. Eixmann, A. Hågård, L. Komguem, S. Kreipl, R.  
31 Matthey, I. Mattis, V. Rizi, J.A. Rodriguez, V. Simeonov, X. Wang, (2004a), Aerosol lidar  
32 intercomparison in the framework of the EARLINET project. 1. Instruments, *Appl. Opt.* 43,  
33 N. 4, 961-976.
- 34 Matthias V., D. Balis, J. Bösenberg, R. Eixmann, M. Iarlori, L. Komguem, I. Mattis, A.  
35 Papayannis, G. Pappalardo, M.R. Perrone and X. Wang, (2004b), Vertical aerosol  
36 distribution over Europe: Statistical analysis of Raman lidar data from 10 European Aerosol  
37 Research Lidar Network (EARLINET) stations, *Journal of Geophysical Research-*  
38 *Atmospheres*, 109, D18, D18201.
- 39 Mattis, I., P. Siefert, D. Müller, M. Tesche, A. Hiebsch, T. Kanitz, J. Schmidt, F. Finger, U.  
40 Wandinger, and A. Ansmann, (2010), Volcanic aerosol layers observed with  
41 multiwavelength Raman lidar over central Europe in 2008–2009, *J. Geophys. Res.*, 115,  
42 D00L04, doi:[10.1029/2009JD013472](http://dx.doi.org/10.1029/2009JD013472).
- 43 Marengo F., B. Johnson, K. Turnbull, S. Newman, J. Haywood, H. Webster and H. Ricketts,  
44 (2011), Airborne lidar observations of the 2010 Eyjafjallajökull volcanic ash plume, *J.*  
45 *Geophys. Res.*, 116, D00U05, doi:10.1029/2011JD016396.



- 1 Mona L., A. Amodeo, M. Pandolfi and G. Pappalardo, (2006), Saharan dust intrusions in the  
2 Mediterranean area: three years of lidar measurements in Potenza, *J. Geophys. Res.*, vol.  
3 111, D16203, doi:10.1029/2005JD006569.
- 4 Mona, L., A. Amodeo, G. D'Amico, A. Giunta, F. Madonna, and G. Pappalardo, (2012), Multi-  
5 wavelength Raman lidar observations of the Eyjafjallajökull volcanic cloud over Potenza,  
6 Southern Italy, *Atmos. Chem. Phys.*, 12, 2229-2244, doi:10.5194/acp-12-2229-2012.
- 7 Moxnes, E. D., N. I. Kristiansen, A. Stohl, L. Clarisse, A. Durant, K. Weber, and A. Vogel (2014),  
8 Separation of ash and sulfur dioxide during the 2011 Grímsvötn eruption, *J. Geophys. Res.*  
9 *Atmos.*, 119, 7477–7501, doi:10.1002/2013JD021129.
- 10 Müller, D., Mattis, I., Ansmann, A., Wandinger, U., Ritter, C., Kaiser, D., (2007),  
11 Multiwavelength Raman lidar observations of particle growth during long-range transport  
12 of forest-fire smoke in the free troposphere. *Geophys. Res. Lett.*, 34, L05803,  
13 2006GL027936.
- 14 Navas-Guzman, F., D. Müller, J. A. Bravo-Aranda, J. L. Guerrero-Rascado, M. J. Granados-  
15 Munoz, D. Perez-Ramirez, F. J. Olmo, and L. Alados-Arboledas, (2013), Eruption of the  
16 Eyjafjallajökull Volcano in spring 2010: Multiwavelength Raman lidar measurements of  
17 sulphate particles in the lower troposphere. *J. Geophys. Res.*, 118, 1804–1813,  
18 doi:10.1002/jgrd.50116.
- 19 Pappalardo G., et al., (2004), Aerosol lidar intercomparison in the framework of the EARLINET  
20 project. 3. Raman lidar algorithm for aerosol extinction, backscatter and lidar ratio, *Appl.*  
21 *Opt.*, 43. N. 28, 53705385.
- 22 Pappalardo G., L. Moma, G. D'Amico, et al., (2013) Four-dimensional distribution of the 2010  
23 Eyjafjallajökull volcanic cloud over Europe observed by EARLINET, *Atmos. Chem. Phys.*, 13,  
24 4429-4450, doi:10.5194/acp-13-4429-2013.
- 25 Pappalardo, G., et al., (2014), EARLINET: towards an advanced sustainable European aerosol  
26 lidar network, *Atmos. Meas. Tech.*, 7, 2389-2409, doi:10.5194/amt-7-2389-2014.
- 27 Papayannis A., et al., (2008), Systematic lidar observations of Saharan dust over Europe in the  
28 frame of EARLINET (2000-2002), *Journal of Geophysical Research*, 113,  
29 doi:10.1029/2007JD009028.
- 30 Papayannis, A., et al., (2012), Optical properties and vertical extension of aged ash layers over  
31 the Eastern Mediterranean as observed by Raman lidars during the Eyjafjallajökull eruption  
32 in May 2010, *Atmospheric Environment*, 48, 56-65,  
33 doi:10.1016/j.atmosenv.2011.08.037.
- 34 Perrone, M. R., De Tomasi, F., Stohl, A., and Kristiansen, N. I., (2012), Integration of  
35 measurements and model simulations to characterize Eyjafjallajökull volcanic aerosols  
36 over south-eastern Italy, *Atmos. Chem. Phys.*, 12, 10001-10013, doi:10.5194/acp-12-  
37 10001-2012.
- 38 Pollack, J., Toon, O. and Khare, B, (1973), Optical properties of some terrestrial rocks and  
39 glasses, *Icarus*, 19, 372-389.
- 40 Prata, A.J. and A.T. Prata, (2012), Eyjafjallajökull volcanic ash concentrations determined using  
41 Spin Enhanced Visible and Infrared Imager measurements, *J. Geophys. Res.*, doi:  
42 10.1029/2011JD016800
- 43 Rix, M., P. Valks, N. Hao, D. Loyola, H. Schlager, H. Huntrieser, J. Flemming, U. Koehler, U.  
44 Schumann, and A. Inness, (2012), Volcanic SO<sub>2</sub>, BrO and plume height estimations using  
45 GOME-2 satellite measurements during the eruption of Eyjafjallajökull in May 2010, *J.*  
46 *Geophys. Res.*, 117, D00U19, doi:10.1029/2011JD016718.



- 1   Sears, T. M., G. E. Thomas, E. Carboni, A. J. A. Smith, and R. G. Grainger (2013), SO<sub>2</sub> as a possible  
2    proxy for volcanic ash in aviation hazard avoidance, *J. Geophys. Res. Atmos.*, 118, 5698–  
3    5709, doi:10.1002/jgrd.50505
- 4   Schumann, U., et al., (2011), Airborne observations of the Eyjafjalla volcano ash cloud over  
5    Europe during air space closure in April and May 2010, *Atmos. Chem. Phys.*, 11, 2245-2279,  
6    doi:10.5194/acp-11-2245-2011.
- 7   Sinyuk, A., Torres, O., and Dubovik, O., (2003), Combined use of satellite and surface  
8    observations to infer the imaginary part of refractive index of Saharan dust, *Geophys. Res.*  
9    *Lett.*, 30, 1081, doi:10.1029/2002GL016189.
- 10   Spinetti C, G. Salerno, T. Caltabiano, et al., (2014), Volcanic SO<sub>2</sub> by UV-TIR satellite retrievals:  
11    validation by using ground-based network at Mt. Etna, *Annals in Geophysics*, Vol 57,  
12    <http://dx.doi.org/10.4401/ag-6641>, Fast Track 2.
- 13   Stohl, A., et al., (2011), Determination of time- and height-resolved volcanic ash emissions and  
14    their use for quantitative ash dispersion modeling: the 2010 Eyjafjallajökull eruption,  
15    *Atmos. Chem. Phys.*, 11, 4333-4351, doi:10.5194/acp-11-4333-2011.
- 16   Thomas, G. E., Poulsen, C. A., Sayer, A. M., Marsh, S. H., Dean, S. M., Carboni, E., Siddans, R.,  
17    Grainger, R. G. and Lawrence, B. N., (2009a), The GRAPE aerosol retrieval algorithm,  
18    *Atmos. Meas. Tech.*, 2, 679-701, doi:10.5194/amt-2-679-2009.
- 19   Thomas, G. E., E. Carboni, A.M. Sayer, et al., (2009b), Oxford-RAL Aerosol and Cloud (ORAC):  
20    aerosol retrievals from satellite radiometers in Satellite Aerosol Remote Sensing Over Land  
21    (Eds: A.A. Kokhanovsky and G. de Leeuw), Springer.
- 22   Torres, O., Bhartia, P. K., Herman, J. R., Ahmad, Z., and Gleason, J., (1998), Derivation of  
23    aerosol properties from satellite measurements of backscattered ultraviolet radiation:  
24    theoretical basis, *J. Geophys. Res.*, 103, D14, <http://dx.doi.org/10.1029/98JD00900>.
- 25   Ventress, L.J.; Carboni, E.; Grainger, R.G.; Smith, A. J. Retrieval of ash optical properties from  
26    IASI measurements. *Atmos. Chem. Phys.*, in prep.
- 27   Volz, F. E., (2009), Infrared optical constants of ammonium sulfate, Sahara dust, volcanic  
28    pumice and fly ash, *Appl. Opt.* 48, 564-568.
- 29   Walker, J. C., Dudhia, A., and Carboni, E., (2011), An effective method for the detection of  
30    trace species demonstrated using the MetOp Infrared Atmospheric Sounding  
31    Interferometer, *Atmos. Meas. Tech.*, 4, 1567-1580, doi:10.5194/amt-4-1567-2011.
- 32   Wang, P., Stammes, P., van der A, R., Pinardi, G., and van Roozendael, M., (2008a), FRESCO+:  
33    an improved O<sub>2</sub> A-band cloud retrieval algorithm for tropospheric trace gas retrievals,  
34    *Atmos. Chem. Phys.*, 8, 6565-6576, <http://dx.doi.org/10.5194/acp-8-6565-2008>.
- 35   Wang, P., O. N.E. Tuinder, L. G. Tilstra, M. de Graaf and P. Stammes, (2012), Interpretation of  
36    FRESCO cloud retrievals in case of absorbing aerosol events, *Atm. Chem. Phys.*,  
37    doi:10.5194/acp-12-9057-2012.
- 38   Wang X., A. Boselli, L. D'Avino, G. Pisani, N. Spinelli, A. Amodeo, A. Chaikovsky, M. Wiegner, S.  
39    Nickovic, A. Papayannis, M.R. Perrone, V. Rizi, L. Sauvage and A. Stohl, (2008b), Volcanic  
40    dust characterization by EARLINET during Etna's eruptions in 2001-2002, *Atmospheric*  
41    *Environment*, 42, 893–905.
- 42   Wandinger, U., et al., (2015), EARLINET instrument intercomparison campaigns: overview on  
43    strategy and results, *Atmos. Meas. Tech. Discuss.*, 8, 10473-10522, doi:10.5194/amt-d-8-  
44    10473-2015.



- 1 Winker, D. M., Z. Liu, A. Omar, J. Tackett, and D. Fairlie (2012), CALIOP observations of the
- 2 transport of ash from the Eyjafjallajökull volcano in April 2010, *J. Geophys. Res.*, 117,
- 3 D00U15, doi:10.1029/2011JD016499.
  
- 4 World Meteorological Organization (2015) WMO SCOPE-Nowcasting: Meeting on the
- 5 Intercomparison of Satellite based Volcanic Ash Retrieval Algorithms, Final Report,
- 6 [http://www.wmo.int/pages/prog/sat/documents/SCOPE-NWC-](http://www.wmo.int/pages/prog/sat/documents/SCOPE-NWC-PP2_VAIntercompWSReport2015.pdf)
- 7 [PP2\\_VAIntercompWSReport2015.pdf](http://www.wmo.int/pages/prog/sat/documents/SCOPE-NWC-PP2_VAIntercompWSReport2015.pdf), last accessed 2/12/2015
  
- 8 Zehner C., Ed. (2010). Monitoring Volcanic Ash from Space. Proceedings of the ESA-EUMETSAT
- 9 workshop on the 14 April to 23 May 2010 eruption at the Eyjafjoll volcano, South Iceland.
- 10 Frascati, Italy, 26-27 May 2010. ESA-Publication STM-280. doi:10.5270/atmch-10-01.
- 11



1 **Figure captions**

2 Figure 1. Characteristics of the FAAM flight of 16-5-2010. The flight track colored with AOD  
3 (a), and the flight altitude versus time in UT along with a time-altitude cross section for the  
4 aerosol extinction coefficient at 355nm (in  $Mm^{-1}$ ) measured with the aircraft lidar (b).

5 Figure 2. Scatter plots between satellite ash optical depth at 550nm and EARLINET ash layer  
6 optical depth at 532nm for GOME-2A (a) and (b), IASI-UOXF (c) and (d) and IASI-ULB (e)  
7 products. Different colors correspond to different European domains. See Table I for more  
8 details.

9 Figure 3. Scatter plots between satellite ash layer height and EARLINET ash layer height (in  
10 km), for GOME-2A (a), and IASI-UOXF (b).

11 Figure 4. Ash optical depth at 550nm and airborne lidar ash layer optical depth at 355 nm as  
12 a function of aircraft time. IASI-UOXF products for the 16<sup>th</sup> of May 2010 (a) and (b), IASI-ULB  
13 products for the 16<sup>th</sup> of May 2010 (c) and GOME-2A product for the 17<sup>th</sup> of May 2010 (d). The  
14 flight tracks for these two days, colored with AOD are shown in (e) and (f)

15 Figure 5. Ash layer height and aircraft lidar ash layer height (in km) 355nm as a function of  
16 aircraft time, GOME-2A for 17<sup>th</sup> of May 2010 (a), and IASI-UOXF for the 16<sup>th</sup> of May 2010 (b).

17

18



1 **Table 1.** Locations of EARLINET lidar stations, their geographical coordinates and corresponding domain  
2 assigned (C: Central Europe, N: North-Central Europe, SW: Iberian Peninsula, SE: Italy-Balkans).

Site	Altitude a.s.l. (m)	Lat. (N)	Long. (E)	Domain
Andøya, Norway	380	69.28	16.01	N
Athens, Greece	200	37.96	23.78	SE
Barcelona, Spain	115	41.39	2.11	SW
Belsk, Poland	180	51.84	20.79	N
Bucharest-Magurele, Romania	93	44.45	26.03	SE
Cabauw, The Netherlands	1	51.97	4.93	N
Evora, Portugal				SW
Garmisch-Partenkirchen, Germany	730	47.48	11.06	C
Granada, Spain	680	37.16	-3.61	SW
Hamburg, Germany	25	53.57	9.97	N
Ispra, Italy	209	45.82	8.63	C
L'Aquila, Italy	683	42.38	13.32	SE
Lecce, Italy	30	40.30	18.10	SE
Leipzig, Germany	100	51.35	12.44	N
Linköping, Sweden	80	58.39	15.57	N
Madrid, Spain	669	40.45	-3.73	SW
Maisach, Germany	515	48.21	11.26	C
Minsk, Belarus	200	53.92	27.60	N
Napoli, Italy	118	40.84	14.18	SE
Neuchâtel, Switzerland	487	47.00	6.96	C
OHP, France	683	43.96	5.71	SW
Palaiseau, France	162	48.70	2.20	N
Payerne, Switzerland	456	46.81	6.94	C
Potenza, Italy	760	40.60	15.72	SE
Sofia, Bulgaria	550	42.67	23.33	SE
Thessaloniki, Greece	60	40.63	22.95	SE

3





1 **Table II.** Collocation criteria examined in the EARLINET-satellite comparisons

Institute	Satellite product	Overpass time	Amount of Data In days	Co-location Criteria	Comments
KNMI	GOME2/MetopA	09:30 LT	14	3h & 300km 5h & 300km 3h & 500km 5h & 500km	
UOXF	IASI/MetopA-Nominal Algorithm	09:30 LT 21:30 LT	18	1h & 100km 3h & 300km	
UOXF	IASI/MetopA-Fast Algorithm	09:30 LT 21:30 LT	19	1h & 100km 1h & 300km 3h & 100km 3h & 300km	3 fixed heights provided, 400 hPa, 600 hPa & 800 hPa
ULB	IASI/MetopA	09:30 LT 21:30 LT	48	1h & 100km 1h & 300km 3h & 100km 3h & 300km	

2

3



1 **Table III.** Collocation criteria examined in the aircraft-satellite comparisons. The flights were  
 2 performed between 13:00 and 17:30 U.T..

Institute	Satellite product	Overpass time	Amount of data in days	Co-location Criteria	Comments
			<b>Max # 5</b>	<b>No time constraint</b>	
KNMI	GOME2/MetopA	09:30 LT	1	100km/200km	
UOXF	IASI/MetopA-Nominal Algorithm	09:30 LT 21:30 LT	4	50/100/200km	
UOXF	IASI/MetopA-Fast Algorithm	09:30 LT 21:30 LT	4	50/100/200km	3 fixed heights provided, 400, 600 & 800mbar
ULB	IASI/MetopA	09:30 LT 21:30 LT	5	50/100/200km	

3

4



1 **Table IV.** Statistical mean values and associated standard deviation for the EARLINET and  
 2 the satellite ash optical depth estimates presented for collocated measurements.

Product	Spatiotemporal criteria	EARLINET mean AOD at 532nm	Satellite mean AOD at 550nm
GOME-2A, KNMI <i>dust</i>	300km & 5h	0.19±0.22	1.29±0.48
GOME-2A, KNMI <i>volz</i>	300km & 5h	0.19±0.22	1.32±0.69
IASI, UOXF nominal	100km & 1h	0.12±0.12	0.08±0.08
IASI, UOXF fast 400hPa	100km & 1h	0.12±0.12	0.10±0.04
IASI, UOXF fast 600hPa	100km & 1h	0.12±0.12	0.17±0.12
IASI, UOXF fast 800 hPa	100km & 1h	0.12±0.12	0.32±0.38
IASI, ULB	100km & 1h	0.14±0.14	0.09±0.07

3

4 **Table V.** Statistical mean values and associated standard deviation for the EARLINET and the  
 5 satellite ash plume height estimates.

Product	Spatiotemporal criteria	EARLINET mean and standard deviation [km]	Satellite mean and standard deviation [km]
IASI, UOXF nominal	100km & 1h	3.63±0.95	3.4±0.78
GOME2/MetOp-A	300km & 5h	3.92±1.22	2.07±1.22

6

7



1 **Table VI.** Statistical mean values and associated standard deviation for the airborne lidar  
 2 and the satellite ash optical depth estimates at 550nm presented for collocated  
 3 measurements.

Institute	Instrument & algorithm	Spatial criteria	Mean Satellite AOD levels	Mean Aircraft AOD Levels	Number of common observations
KNMI	GOME-2/MetOp-A	200km	0.42±0.03	0.23±0.15	64
UOXF	IASI/MetopA Nominal Algorithm	50km	0.28±0.25	0.19±0.16	787
UOXF	IASI/MetopA Fast Algorithm 400hPa	50km	0.20±0.30	0.19±0.16	776
UOXF	IASI/MetopA Fast Algorithm 600hPa	50km	0.23±0.29	0.18±0.15	740
UOXF	IASI/MetopA Fast Algorithm 800hPa	50km	0.30±0.40	0.18±0.16	732
ULB	IASI/MetopA	50km	0.21±0.15	0.25±0.17	463

4

5

6 **Table VII.** Statistical mean values and associated standard deviation for the airborne lidar  
 7 and the satellite ash plume height estimates.

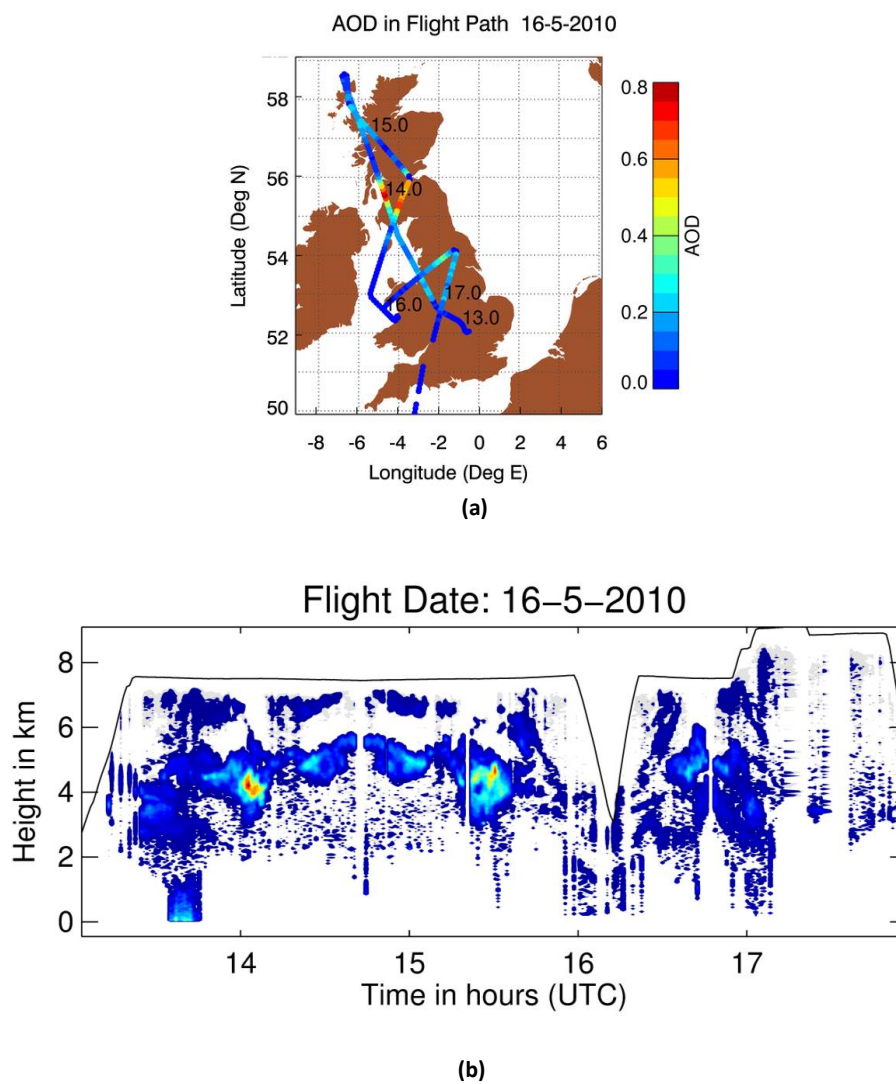
Product	Spatial criteria	Aircraft mean and standard deviation [km]	Satellite mean and standard deviation [km]
IASI/MetOpA, UOXF nominal	50km	4.30±2.00	3.73±1.45
GOME-2-MetOpA, KNMI	200km	3.87±1.70	5.62±0.54

8

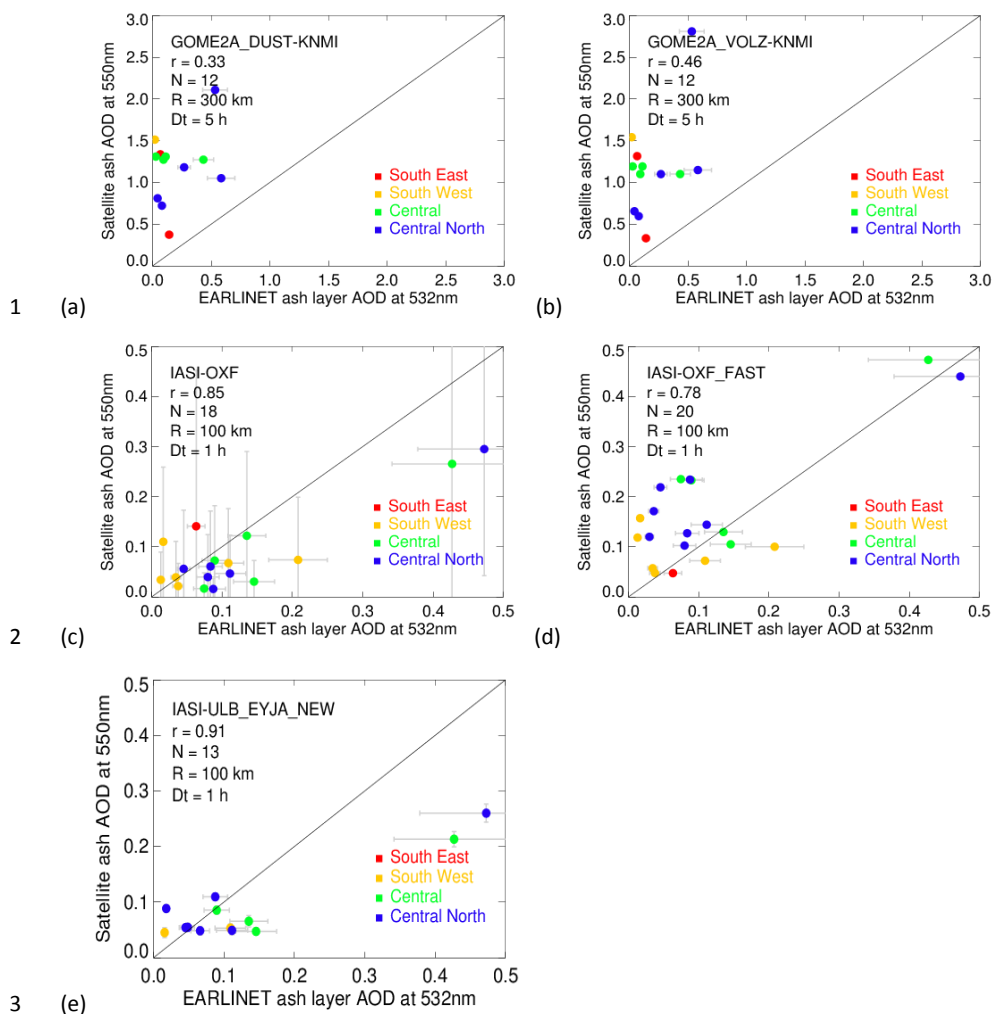
9



1



2 **Figure 1.**



4 **Figure 2.**

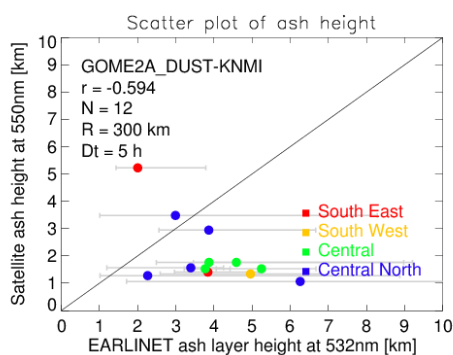
5

6

7

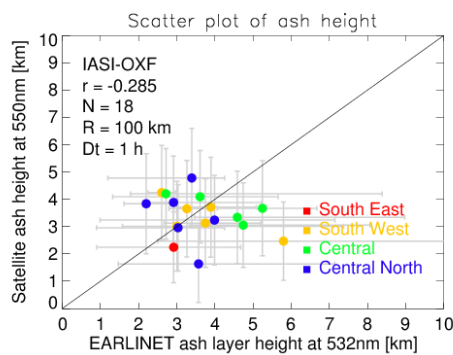


1



2

(a)



3

(b)

4 **Figure 3.**

5

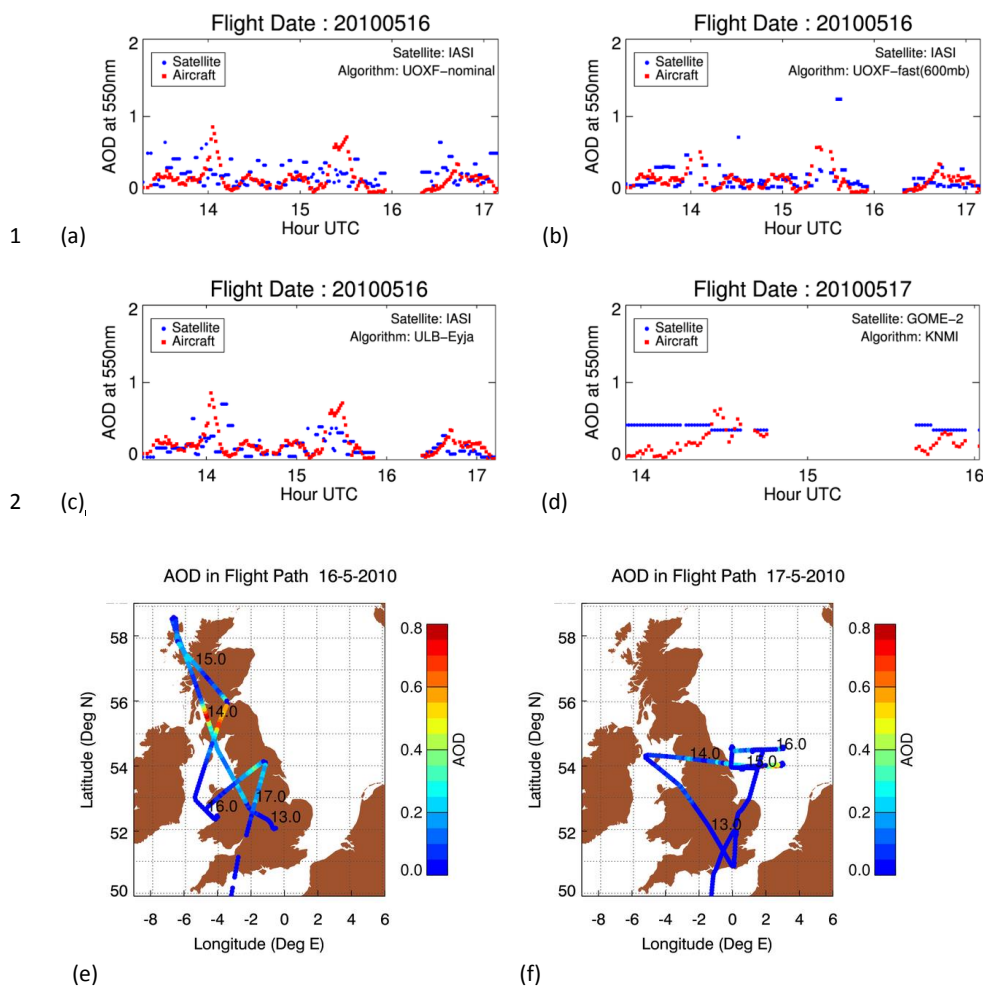
6

7

8

9

10



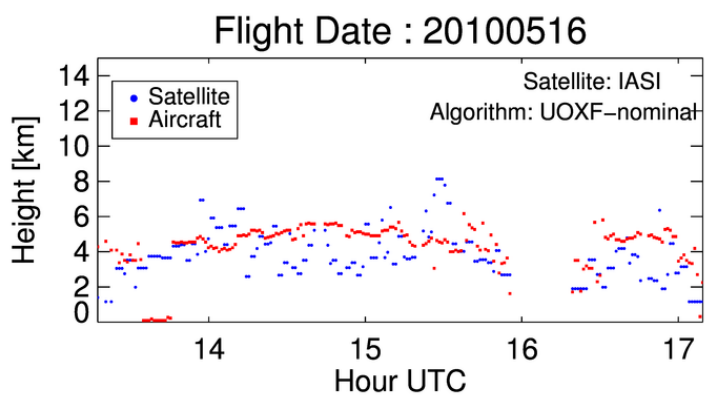
3 **Figure 4.**

4

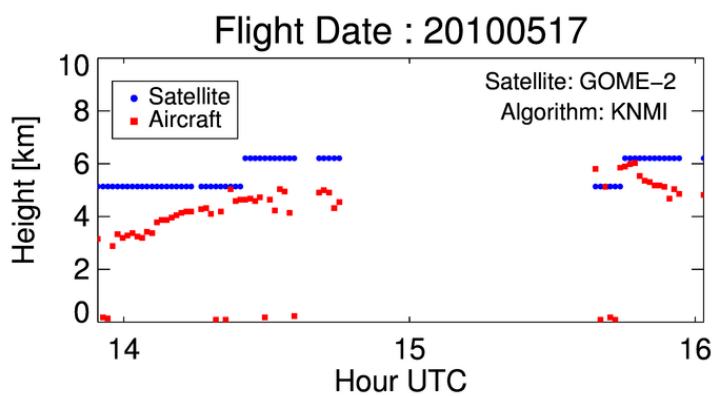




1



2 (a)



3 (b)

4 **Figure 5.**

5

6

7

8

9

10